Flashing flexodomains and electroconvection rolls in a nematic liquid crystal

Péter Salamon,[1] Nándor Éber,[1] Alexei Krekhov,[2] and Ágnes Buka[1]

[1]*Institute for Solid State Physics and Optics, Wigner Research Centre for Physics, Hungarian Academy of Sciences, H-1525 Budapest, P.O.B.49, Hungary*

[2]*Institute of Physics, University of Bayreuth, D-95440 Bayreuth, Germany*

(Received 10 February 2013; revised manuscript received 4 March 2013; published 20 March 2013)

Pattern forming instabilities induced by ultralow frequency sinusoidal voltages were studied in a rodlike nematic liquid crystal by microscopic observations and simultaneous electric current measurements. Two pattern morphologies, electroconvection (EC) and flexodomains (FD), were distinguished, both appearing as time separated flashes within each half period of driving. A correlation was found between the time instants of the EC flashes and those of the nonlinear current response. The voltage dependence of the pattern contrast $C(U)$ for EC has a different character than that for the FD. The flattening of $C(U)$ at reducing the frequency was described in terms of an imperfect bifurcation model. Analyzing the threshold characteristics of FD, the temperature dependence of the difference $|e_1 - e_3|$ of the flexoelectric coefficients was also determined by considering elastic anisotropy.

DOI: 10.1103/PhysRevE.87.032505 PACS number(s): 61.30.Gd, 47.54.−r

I. INTRODUCTION

Nematic liquid crystals are the simplest paradigm for anisotropic fluids, i.e., liquids with a preferred direction of the orientation of molecules with anisotropic shape which is described by the director field **n**. The anisotropy of their dielectric properties allows controlling the director by electric fields. The (usually homogeneous) reorientation of the director by a properly applied voltage changes the direction of the optical axis and hence the light transmittance of the sample; this forms the physical background of the liquid crystal displays, [1] used widespread in common electronic devices.

Applying an electric voltage to a nematic liquid crystal layer can, however, often result in the appearance of spatiotemporal, periodic, or disordered structures too. The conditions of their occurrence, the pattern morphologies, and their onset characteristics have been extensively studied for decades, both experimentally and theoretically [1–14].

In the mostly studied planar configuration, where the director is initially oriented parallel to the confining plates, one of the electric field induced patterns corresponds to spatially periodic, equilibrium director deformations (seen as stripes parallel to the director in a polarizing microscope), occurring due to a flexoelectric free energy gain of the deformed state; therefore, they have been coined *flexoelectric domains* (FDs) [2]. FDs have so far been detected in a few nematic compounds only and they are observable at dc (or very low frequency dc) driving only.

A more frequent, but also more complex, pattern forming phenomenon is the electroconvection (EC), where the director distortions are accompanied by space charge separation and hence by material flow, thus having a dissipative character. It could be observed in many nematics, some of which possess substantially different material properties [3,4]. EC patterns could be induced in a wide frequency range of the applied voltage (ranging from dc up to several hundreds kHz ac); the resulting convection rolls are seen in a polarizing microscope as stripes whose direction may be normal, to oblique, or parallel with the director. Up to now, studies were mostly focused on the class of nematics with negative dielectric and positive conductivity anisotropies and on driving frequencies f within the range of 10 Hz to 10 kHz. In this f range, evolution of the pattern requires numerous driving periods after voltage application. For such conditions, the variation of pattern morphologies (conductive and dielectric regimes, oblique and normal rolls) upon the amplitude and frequency of the applied voltage has been explored in detail and the mechanism as an electrohydrodynamic instability has been well understood. A quantitative theoretical description of the pattern threshold, the critical wave vector, and some secondary transitions (e.g., abnormal rolls) could be given combining nematodynamics with electrodynamics under the simplifying assumption of Ohmic conductivity (now called as the standard model of EC [5]) or via its extensions by flexoelectricity [6] or by ionic diffusion and recombination [7].

Recently, interest has arisen to study the behavior in another, subhertz frequency, range where the pattern growth and decay times are (much) shorter than the driving period, using compounds which may exhibit both EC and FD patterns. It has been proven experimentally that at such ultralow frequencies both for the dielectric [8] and the conductive [9] EC regimes, as well as for the FD [8,9], the patterns are flashing, i.e., they exist only in a small part of the driving period. It has been found that there is an f range ($\sim$1–100 mHz) where both EC and FD patterns can exist in each driving half period in the form of successive (time shifted) flashes. Theoretical calculations based on the standard model of EC extended with flexoelectricity [6] (which is able to describe FDs too [10]) have justified that flashing patterns are indeed the solutions of the nematoelectrohydrodynamic equations at ultralow f. The calculated position of the FD flashes within the driving half period showed quantitative matches with the experiments, while for the position of the EC flashes the frequency dependence was only qualitatively reproduced by the calculations, as the EC flashes come earlier within the period than expected [9].

In this paper, we present further experimental results on the ultralow f behavior, however, in a different system than those reported before. The paper is organized as follows. Section II introduces our compound and the experimental method. The

new findings are grouped around three subtopics: Section III A reports on the temporal evolution of the patterns within the period, Sec. III B deals with the frequency dependence of the threshold characteristics, and Sec. III C provides data on the temperature dependence of various material parameters. Finally, the paper is concluded in Sec. IV with a summary and some closing remarks.

II. EXPERIMENT

Our measurements have been performed on the nematic liquid crystal 4-n-octyloxyphenyl 4-n-methyloxybenzoate (1OO8) [1] that shows only a nematic mesophase. The chemical structure of 1OO8 is shown in Fig. 1.

In heating, it melts to nematic from the crystalline phase at 63.5 °C, while the clearing point (T_{NI}) equals to 76.7 °C. The nematic phase can be supercooled down to 53 °C. The material parameters of 1OO8, such as the dielectric anisotropy ($\varepsilon_a = \varepsilon_\parallel - \varepsilon_\perp$), the optical anisotropy ($n_a = n_\parallel - n_\perp$), the anisotropy of the diamagnetic susceptibility ($\chi_a = \chi_\parallel - \chi_\perp$), and the bulk elastic constants (K_{11}, K_{22}, K_{33}) were determined as the function of temperature using a method based on magnetic and electric Freedericksz transitions [15]. Here, ε and n denote the dielectric permittivity and the refractive index, respectively; the subscripts $\parallel$ and $\perp$ correspond to measurement directions parallel with and perpendicular to the director.

The compound was investigated in commercial sandwich cells (E.H.C. Co.) with ITO electrodes coated with rubbed polyimide layers for planar alignment. The electrode area was 1 cm^2. The thickness of the empty cells ($d = 10.4$–10.8 μm) was measured by an Ocean Optics spectrophotometer. During the measurements, the temperature of the sample was kept constant within 0.01 °C in an Instec HSi heat stage controlled with an mK-1 board. The sample was driven by a sinusoidal voltage $\tilde{U}(t)$ of an Agilent 33120A function generator via a high-voltage amplifier: $\tilde{U}(t) = \sqrt{2}U \sin(2\pi f t)$.

The electric field induced patterns were observed by a Leica DM RX polarizing microscope in transmission mode with white light illumination using the shadowgraph technique [17] (the polarizer was removed, while the analyzer was set to be parallel with the rubbing direction). The imaging system was equipped with an EoSens MC1362 high speed camera interfaced by an Inspecta-5 frame grabber. After waiting one or two periods of the driving signal following the application of the voltage to the sample (or waiting 5 s at frequencies higher than 0.2 Hz), a sequence of 1000 images was recorded. The acquisition of the first image was triggered by the zero crossing (from negative to positive) of the applied voltage.

In addition to the optical observations, the electric current through the cell was monitored by measuring the voltage drop on a relatively small, known resistance connected in series with the sample. Simultaneously, the driving waveform was also recorded by a TiePie Handyscope HS3 oscilloscope. The data acquisition and processing system was fully automated.

[1] Two abbreviation styles are known in the literature for the members of the 4-n-alkyloxyphenyl 4-n-alkyloxybenzoate homologous series. Here, we have adopted the one used by Nair *et al.* [16]. According to the alternative style by Kochowska *et al.* [13], the same compound could also be abbreviated as $\frac{1}{8}$.

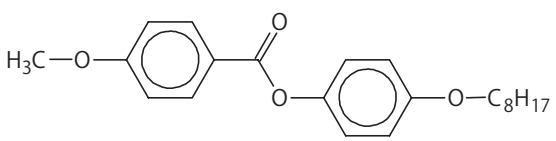

FIG. 1. The chemical structure of the rodlike nematic molecule 4-n-octyloxyphenyl 4-n-methyloxybenzoate (1OO8).

III. RESULTS AND DISCUSSION

A. Flashing contrast and current

Applying a low frequency (e.g., $f = 50$ mHz) sinusoidal voltage to the cell, patterns appear above a threshold voltage in a narrow time window in each half period of driving. Two distinct pattern morphologies were found with different thresholds, similarly to previous observations on other nematics [9]. Representative snapshots of the patterns and their two-dimensional (2D) Fourier transforms (the spectral intensities) are presented in Fig. 2. The two morphologies can be attributed to oblique conductive EC rolls [a zigzag pattern, Fig. 2(a)] and to flexodomains [Fig. 2(b)]; the latter appear as stripes parallel to the initial director alignment.

For a quantitative analysis of the pattern evolution, it is necessary to provide a proper definition for the pattern contrast, which has a minimum (ideally zero) in the homogeneous state and increases as the pattern emerges. A common procedure is to perform a 2D Fourier transformation of the images in order to find the critical wave vector $\mathbf{q_c} = (q_x, q_y)$ of the pattern (where the Fourier amplitudes have maxima) and to define the contrast C_q as the sum of the spectral intensities in a region around $\mathbf{q_c}$. It is clear from Fig. 2 that the two pattern types

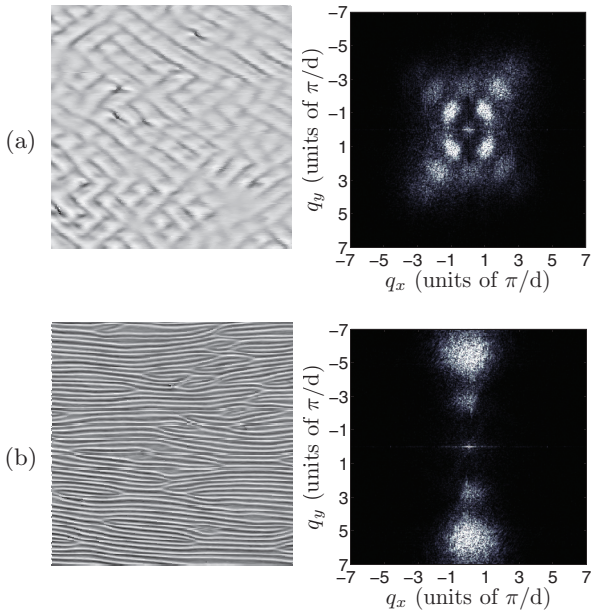

FIG. 2. Snapshot images and their 2D Fourier transforms (a) for electroconvection and (b) for flexodomains at $f = 50$ mHz and $U = 19$ V. The images cover 200 μm × 200 μm area. The initial director orientation lies horizontally.

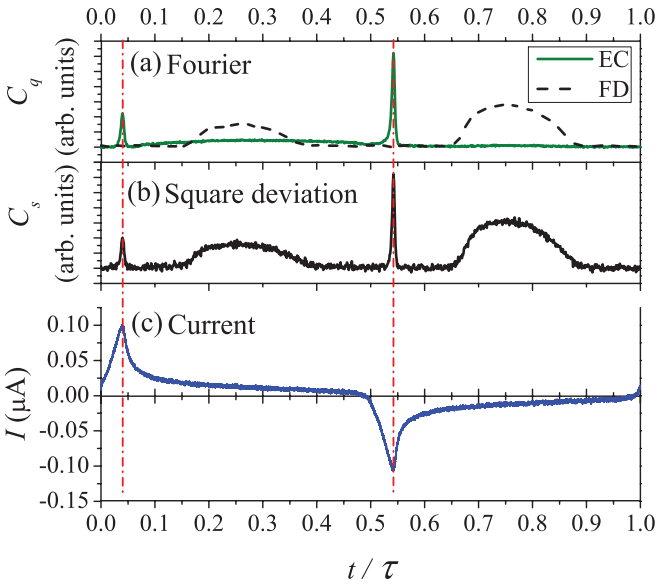

FIG. 3. (Color online) The time dependence within a driving period (a) for the contrast C_q obtained by Fourier technique; (b) for the contrast C_s calculated from the square deviation; and (c) for the electrical current I through the liquid crystal. $t = 0$ corresponds to the zero crossing (from positive to negative) of the applied voltage. The dashed-dotted lines show that the peaks of EC and of the current coincide.

observed in 1OO8 (EC and FD) are characterized by different $\mathbf{q_c}$ vectors, i.e., they are well separated in the Fourier space. Therefore, this contrast definition allows distinguishing them not only from the initial homogeneous state, but also between each other.

Alternatively, a mean square deviation of the image intensities $C_s = \langle(\Phi - \langle\Phi\rangle)^2\rangle$ may also serve as a measure of the contrast. Here, Φ is the intensity of an individual pixel and $\langle\ldots\rangle$ denotes averaging over the whole image. This definition is simpler, although it has the disadvantage of not being able to distinguish various pattern morphologies. Actually, C_s would coincide with C_q if the summation of the spectral intensities were extended over the whole Fourier space.

Figure 3 exhibits and compares the time dependence of contrast within a driving period for both definitions given above, measured in a $d = 10.4$ μm thick cell at $T - T_{NI} = 21.7$ °C driven by an $f = 22$ mHz, $U = 18$ V voltage. Figure 3(a) shows C_q obtained by the Fourier method for the EC (solid line) and the FD (dashed line) patterns. Both curves exhibit a single peak in each half period, but at different time intervals; hence, these two pattern types are well separated not only in the Fourier space, but in time as well. In Fig. 3(b), the contrast C_s calculated by the square deviation is plotted. This curve has two, well separated peaks per half period [looks similar to the superposition of the two curves in Fig. 3(a)], thus can also be used to detect the appearance of both pattern types. Therefore, for simplicity, in the following we will use C_s as the measure of the contrast of the patterns.

Figure 3(c) depicts the time dependence of the electrical current which was measured simultaneously with image acquisition. At this f and U, the current is highly nonlinear; it can be characterized by sharp peaks rather than by a harmonic response. It can be deduced from the figure that, surprisingly, the location of the maxima of the current peaks coincide precisely with the contrast peaks corresponding to the EC flashes (see the dashed-dotted vertical lines in Fig. 3). Numerous different voltages, frequencies, and temperatures were tested. Although at various conditions the time instant of the EC flash may change [9], it still equals to that of the current peak; thus, we can conclude that this is not an accidental coincidence. We suggest that the current spikes trigger the emergence of the EC pattern. Therefore, it appears earlier within the half period (a phase-locking behavior) than expected otherwise.

We note that the spiky behavior of the current is not a consequence of the appearance of the EC pattern. Current spikes have been detected at low voltages (much below any pattern threshold) where no patterns are observable and also in the isotropic phase. We think that the nonlinear current behavior is due to ionic effects and to the presence of insulating polyimide orienting layers on the electrode surfaces of the cell. The presence of (relatively low) concentration of ionic impurities in the nematic makes it to behave as a weak electrolyte. In the studied ultralow frequency range, the current due to the linear impedance of the cell (i.e., the capacitive and the Ohmic components) is at least an order of magnitude smaller than the transient currents due to building or destroying the Debye screening layers near the electrodes; the latter occurs at each polarity reversal of the voltage.

In order to describe the behavior of weak electrolytes in electric fields, several models were developed, differing in their sets of assumptions [18–26], i.e., they take into consideration different subsets of the possible effects listed below: generation and recombination of ions; different mobilities, diffusion coefficients and charges of ionic species; surface adsorption; charge injection; chemical reactions; voltage attenuation due to the orienting layers; etc. Due to the complexity of the models, they mostly focused on the linear response and calculated the low frequency complex impedance which could be compared to low f dielectric spectroscopy data.

Recently, theoretical calculations of the nonlinear current characteristics in response to a low frequency sinusoidal voltage driving were also reported [18,19], yielding curves similar to those shown in Fig. 3(c), however, without comparison with experiments. This gives the hope that after measurements or intelligent guesses of the unknown material parameters of the model, the measured current response can be reproduced; it is remaining a task for the future.

The nematic being a weak electrolyte has consequences on the pattern formation processes. It was shown that the weak electrolyte model (WEM) of EC [7], which considers ionic dissociation and recombination, can account for the traveling of EC roll patterns found occasionally at frequencies above a few tens of Hz. This model has not yet been analyzed for low driving frequencies; due to its high complexity, it remains a challenge for the future to decide whether it is able to describe the phase locking of EC flashes to current spikes.

B. Threshold characteristics

Flexodomains and electroconvection both are threshold phenomena, i.e., the patterns with a critical wave number

$q_c = |\mathbf{q_c}|$ occur above a threshold voltage U_c. Determination of U_c and q_c is therefore the primary task at pattern characterization. At high frequencies ($f > 10$ Hz) for $U > U_c$, patterns usually develop within seconds; therefore, thresholds can easily be estimated by increasing U as the voltage at which the pattern becomes perceptible by eyes in the microscope. This simple technique practically does not work at our ultralow frequency driving since the driving period is quite long and in addition the patterns appear as flashes, which means they can be observed only in a short time window.

In order to determine U_c precisely, one has to follow quantitatively the emergence of patterns from the homogeneous state, i.e., to record and then analyze the contrast-voltage curves. As the contrast varies within the driving period [as shown in Fig. 3(b)], the maximum C_m of the contrast C_s in the FD (or EC) peak can be regarded as a measure to what extent the FD (or EC) pattern has been developed at a given applied voltage.

In an ideal case (perfect bifurcation), the contrast C_m should be zero at voltages below the threshold. Experimentally, a nonzero background contrast C_b is always found even in the homogeneous state at no applied voltage [$C_b = C_s(U = 0)$]. This background contrast comes from various sources: the electronic noise of the camera, the thermal fluctuation of the director in a planar nematic, imperfections of the orientation or inhomogeneity of the illumination. This background was automatically subtracted from each data point; thus, it will not be indicated in the forthcoming figures.

As the voltage is increased above U_c, the initial planar director orientation $\mathbf{n}_0 = (1,0,0)$ becomes unstable and a spatially periodic director distortion $\delta\mathbf{n} = \mathbf{n}_{\rm lin} A \exp[i(q_x x + q_y y)]$ appears. Here, $\mathbf{n}_{\rm lin} = (0,n_y,n_z)$ is a linear eigenvector, $A \propto \sqrt{U^2 - U_c^2}$ characterizes the amplitude of the distortion, and $\mathbf{q_c} = (q_x,q_y)$ is the wave vector of the pattern. The spatially periodic director distortion results in a shadowgraph image whose intensity modulation I_s depends on the amplitude of the vertical distortion An_z. For small distortion amplitudes (not too far from threshold), the intensity modulation in the leading order is given [27] by $I_s = c_a A + c_p A^2$ with the first order amplitude term and the second order phase term. For EC patterns [normal rolls with $\mathbf{q_c} = (q_x,0)$], the linear term is dominating and $I_s \propto A$. In case of FD, where $\mathbf{q_c} = (0,q_y)$, the relevant contribution to the shadowgraph intensity is of the second order [28]: $I_s \propto A^2$. The contrast of the shadowgraph image defined as the mean square deviation of the image intensities is then $C_s \propto I_s^2$. Thus, the maximum of the contrast within the driving period is expected to be $C_{m\rm EC} \propto (U^2 - U_{c\rm EC}^2)$ for an EC pattern and $C_{m\rm FD} \propto (U^2 - U_{c\rm FD}^2)^2$ for the FD [8]. In the vicinity of the threshold $(U^2 - U_{c\rm FD}^2) \approx 2U_c(U - U_c)$, therefore $C_{m\rm EC}$ as well as $\sqrt{C_{m\rm FD}}$ should grow linearly with the voltage.

Figure 4 shows the measured $\sqrt{C_{m\rm FD}}(U)$ curves for a few frequencies. It is seen that the linear relation near the threshold is obeyed quite well, although the transition is smeared a little (due to imperfections and/or the occurrence of subcritical fluctuations). Therefore, the threshold voltage $U_{c\rm FD}$ is actually determined by a linear extrapolation, as the intersection of the horizontal axis with the line fitted onto the linear section of the $C_m(U)$ curve slightly above the suspected threshold. This procedure is going to be referred to as method A.

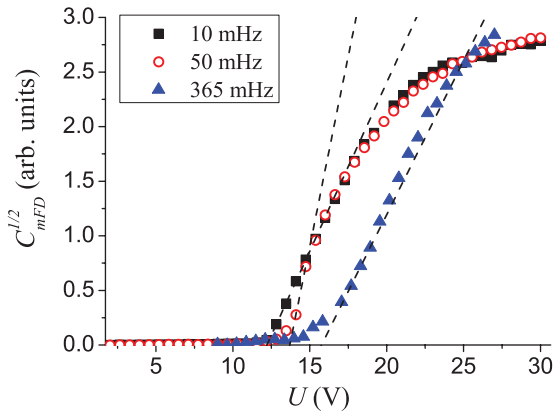

FIG. 4. (Color online) The voltage (rms) dependence of the square root of the FD contrast peaks for different frequencies (symbols). The dashed lines indicate the linear extrapolation.

The voltage dependence of $C_{m\rm EC}$ for EC is shown in Fig. 5 for several driving frequencies. It is clearly seen that the frequency affects not only the threshold voltages, but also the character (the shape) of the $C_{m\rm EC}(U)$ curves. Evidently, the linear relation holds only at high frequencies; there, the thresholds $U_{c\rm EC\,A}$ can be determined by extrapolation (method A).

Below 1 Hz, however, there is no sharp increase of the contrast; the $C_m(U)$ curves show rather a slow gradual increase, while the contrast levels and thus the visibility of the patterns vary in the same range as at high frequencies. The determination of thresholds is then not so straightforward. In the absence of a well defined linear part of the contrast curve, method A becomes unreliable; the choice of points used for the extrapolation (the dashed lines in Fig. 5) is to some extent arbitrary.

An alternative way (method B) is to select (arbitrarily) a critical contrast value C_0 (the dashed-dotted line in Fig. 5) where the EC pattern is visible by eye. The voltage $U_{c\rm EC\,B}$, where $C_{m\rm EC}(U_{c\rm EC\,B}) = C_0$, can be regarded as another estimate of the threshold. In the case of forward bifurcations, which the standard EC pattern formation is an example for, the contrast increases continuously from zero. Therefore, $U_{c\rm EC\,B}$ slightly overestimates the threshold.

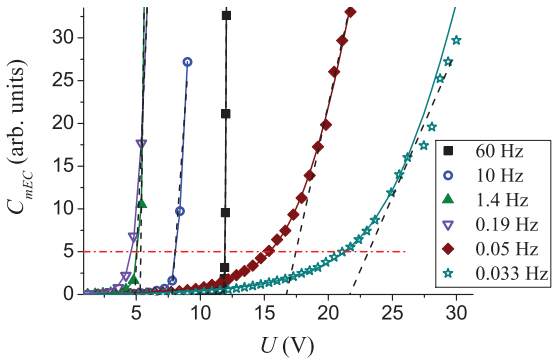

FIG. 5. (Color online) The voltage (rms) dependence of the contrast peaks C_m of EC for different frequencies (symbols). Solid lines are fits with the imperfect bifurcation model, the dashed lines indicate the linear extrapolation.

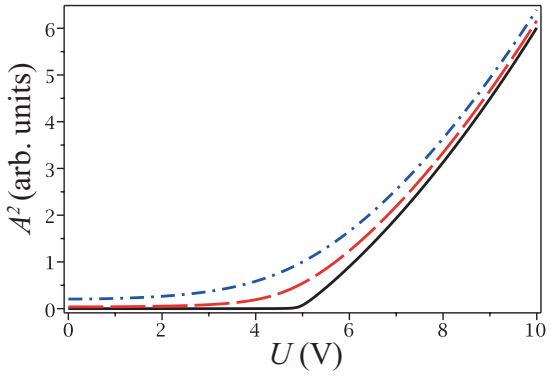

FIG. 6. (Color online) Square of the pattern amplitude A^2 as a function of the applied voltage U for $\delta = 0.01$ (solid line), $\delta = 0.2$ (dashed line), and $\delta = 0.5$ (dotted-dashed line). $U_{c\mathrm{EC}} = 5$, $g = 0.5$.

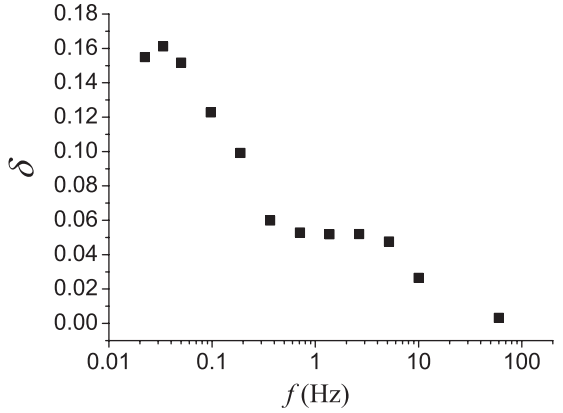

FIG. 7. Frequency dependence of the imperfection parameter δ.

The change in the shape of the $C_{m\mathrm{EC}}(U)$ curves may be interpreted so that the nearly perfect bifurcation (at high f) becomes imperfect at lower f. For an imperfect bifurcation, the amplitude of the director distortion A satisfies the equation

$$\varepsilon A - gA^3 + \delta = 0. \tag{1}$$

Here, $\varepsilon = U^2/U_{c\mathrm{EC}}^2 - 1$, U is the rms applied voltage, $U_{c\mathrm{EC}}$ is the threshold voltage, $g > 0$ characterizes the saturation of the amplitude, and $\delta \geqslant 0$ is the measure for the imperfection ($\delta = 0$ corresponds to the perfect forward bifurcation). For $g > 0$ and $\delta > 0$, only one of the three solutions of Eq. (1) is stable in the whole range of $\varepsilon > -1$ and thus relevant; it reads as

$$\begin{aligned} A &= \left(\frac{\delta}{2g}\right)^{1/3} F(\tilde{\varepsilon}), \\ F(\tilde{\varepsilon}) &= \left(\frac{\tilde{\varepsilon}}{\hat{f}(\tilde{\varepsilon})} + \hat{f}(\tilde{\varepsilon})\right) \quad \text{for} \quad \tilde{\varepsilon} \leqslant 1, \\ F(\tilde{\varepsilon}) &= 2\sqrt{\tilde{\varepsilon}} \cos\left(\frac{1}{3}\arctan\left(\sqrt{\tilde{\varepsilon}^3 - 1}\right)\right) \quad \text{for} \quad \tilde{\varepsilon} > 1, \\ \tilde{\varepsilon} &= \frac{2}{3}\frac{\varepsilon}{(2g\delta^2)^{1/3}}, \ \hat{f}(\tilde{\varepsilon}) = (1 + \sqrt{1 - \tilde{\varepsilon}^3})^{1/3}. \end{aligned} \tag{2}$$

As mentioned above, the maximum contrast $C_{m\mathrm{EC}}$ of the EC patterns observed using the shadowgraph technique is proportional to A^2. In Fig. 6, the dependence of A^2 on the applied voltage U is shown for different values of the imperfection parameter δ at fixed values of $U_{c\mathrm{EC}}$ and g. It demonstrates that the shape of the curve changes substantially if the imperfection (δ) increases.

For a precise quantitative analysis, we can use the same background subtraction here, just as was done with the experimental data; therefore, the contrast depicted in Fig. 5 will be related to the amplitude as

$$C_{m\mathrm{EC}} = C_{\max} - C_b = \alpha[A^2(U) - A^2(U = 0)], \tag{3}$$

where $C_{\max}$ is the maximum contrast of the pattern, C_b is the background contrast at $U = 0$, and $\alpha > 0$ is a scaling factor. By combining Eqs. (2) and (3), one can fit the experimental $C_{m\mathrm{EC}}(U)$ curves by this phenomenological model for imperfect bifurcation using four parameters: α, g, δ, and $U_{c\mathrm{EC}}$ (method C).

The actual value of the scaling parameter α is determined by the optical setup and the optical properties. As q_c of the EC pattern depends weakly on f, we can assume that α is frequency independent. Its value could be obtained from the fit at $f = 60$ Hz, leaving only three free parameters for the fits at lower frequencies.

The results of the fit procedure are shown by solid lines in Fig. 5. The match with the experimental data is quite convincing. The frequency dependence of the imperfection parameter δ is plotted in Fig. 7. It clearly shows (what we have already expected from the experimental data in Fig. 5) that the imperfection grows at lower frequencies. Several reasons could be responsible for the increase of the apparent imperfection.

In planar samples aligned by rubbed polyimide layers, a small director pretilt at the confining plates is practically unavoidable. Such pretilt is known to yield imperfect bifurcation (i.e., lack of a sharp threshold) in the case of splay Freedericksz transition. The effect of a tilted alignment on the EC characteristics has theoretically been studied only for high frequencies [29], the pretilt modified U_c, but did not affect the sharpness of the threshold, which is in agreement with our observations (Fig. 5) at high f.

Decreasing the frequency of the applied ac voltage well below the inverse director relaxation time may, however, alter the situation as one enters the regime of quasistatic director response. Here, a small pretilt may enhance the director deformations and correspondingly the contrast of the pattern can develop already at lower voltage amplitudes compared to the high frequency case. Unfortunately, a detailed theoretical analysis of this regime in the presence of pretilt is not yet available.

The nonlinear electric current characteristics presented in Sec. III A may provide another reason for the apparent softening of the ultralow f EC thresholds. The coincidence of the electric current peaks and the EC flashes clearly shows the strong correlation between pattern formation and ionic phenomena: the massive ionic flow helps the electrohydrodynamical instability to emerge. The spatial distribution of the current is not necessarily uniform, mainly due to surface inhomogeneities (which may originate, e.g., from crystallization of the compound) or small variations in the cell thickness and/or pretilt. The current inhomogeneities may locally reduce the threshold of EC. In fact, this effect has been observed: the EC pattern first appears in germs and extends

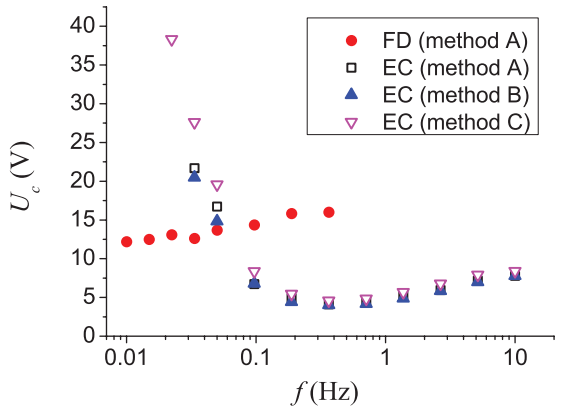

FIG. 8. (Color online) The frequency dependence of threshold voltages (rms) of EC and FD determined by various methods.

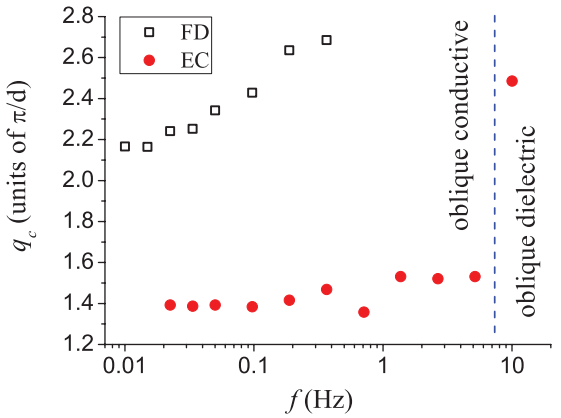

FIG. 9. (Color online) The frequency dependence of the threshold wave numbers for EC and FD.

gradually to larger areas by increasing the voltage. The location of these germs can be identified even in the well developed pattern as small spots or patches of higher contrast [a few such spots can be seen in Fig. 2(a)]. The contrast $C_{m\mathrm{EC}}(U)$ of the pattern plotted in Fig. 5 is calculated over the whole image; thus, a continuous increase of the area filled with pattern leads to a continuous increase of $C_{m\mathrm{EC}}(U)$. Consequently, a locally sharp transition yields a softened, gradual contrast variation. While ionic effects are mostly negligible at high frequencies (linear current response), they become crucial at ultralow frequencies (spiky current response), which may explain the increase of the imperfection parameter for $f \to 0$.

We note that the formation of flexodomains is not affected by the electric current spikes as they occur in different time windows. Therefore, the above scenario of germ-induced pattern evolution does not apply to FD, i.e., the onset of FD remains sharp over the full frequency range of its existence, as shown in Fig. 12.

The frequency dependence of the threshold voltages of both patterns can be seen in Fig. 8. It depicts the $U_{c\mathrm{EC}}$ values determined by all three methods introduced above. The data by methods A (extrapolation) and B (comparison) almost coincide, while the thresholds obtained from fitting to the imperfect bifurcation model are significantly larger at lower frequencies. This is not surprising since methods A and B intrinsically assume that no deformation exists below a threshold, while an imperfect bifurcation actually means a thresholdless deformation with U_c being a parameter only.

Otherwise, the $U_{c\mathrm{EC}}(f)$ curve exhibits the expected behavior. The reduction of the threshold at lowering f in the $0.5 < f < 10$ Hz range corresponds to the theoretical predictions and matches the behavior of other nematics [30]. The increase of $U_{c\mathrm{EC}}$ toward ultralow frequencies is attributed to the internal attenuation due to the insulating polyimide alignment layers on the electrodes [9]. The frequency dependence of $U_{c\mathrm{FD}}$ seems to be significantly weaker than that of $U_{c\mathrm{EC}}$ in the same f range. Taking into account the internal attenuation, the actual FD threshold voltage (on the liquid crystal layer) grows much stronger with f than the apparent threshold plotted in the figure (the voltage applied to the cell), which is in agreement with the theoretical predictions [10].

Figure 8 clearly shows that the two distinct patterns, EC and FDs, coexist in a relatively wide ($0.02\ \mathrm{Hz} < f < 0.4$ Hz) range, even though their threshold voltages are quite different. This is possible because they remain separated in time until the half period of driving voltage is large enough for both patterns to emerge and decay; thus, they can build up from the same almost homogeneous initial state. For $f > 0.4$ Hz, however, this does not hold any more. In that range, aside from the shorter period time, $U_{c\mathrm{EC}}$ is much lower than $U_{c\mathrm{FD}}$. Thus, the EC contrast spikes become much broader and the EC pattern does not decay fully before FD should emerge. Under such conditions, the FD pattern (which has a lower contrast than EC) can not be recognized any more.

As the frequency is reduced, at around 0.05–0.07 Hz, there is an intersection of the two threshold curves ($U_{c\mathrm{FD}}$ and $U_{c\mathrm{EC}}$). At f below this intersection, the threshold of FDs is lower than that of EC; thus, upon increasing the voltage FD is the first instability EC sets on at a higher voltage. This is in accordance with the finding that when applying a pure dc voltage, no EC pattern, only FDs can be detected.

Characterization of the threshold behavior is incomplete without addressing the frequency dependence of the critical wave number $q_c = |\mathbf{q_c}|$. Figure 9 exhibits the relevant curves both for EC (q_{EC}) and FD (q_{FD}). The values were determined using the 2D fast Fourier transformation (FFT) of images taken slightly above the threshold, at $U = 1.05U_c$, in order to have sufficient contrast for the evaluation. Note that for the oblique EC rolls $q_{\mathrm{EC}} = \sqrt{q_x^2 + q_y^2}$, while FDs are parallel to the initial director, so $q_{\mathrm{FD}} \approx q_y$. The wave numbers increase for both patterns with the frequency. In the case of FD, there is a moderate f dependence even at ultralow frequencies. For EC, the change of q_{EC} seems to be very small until 5 Hz. Between 5 and 10 Hz, however, the wave number increases suddenly, which is attributed to the transition between oblique conductive and oblique dielectric EC. To our knowledge, no such transition was reported before in the literature. We note that the obliqueness angle decreases with the frequency, and the Lifshitz point is reached in the dielectric regime at $f_L \approx 80$ Hz.

C. Temperature dependence of the flexoelectric coefficients

Although several experimental methods have been proposed to measure the flexoelectric coefficients, measurements

usually can not be done without serious compromises [14]. Analysis of the threshold parameters (q_{cFD}, U_{cFD}) of the flexoelectric instability is one of the possible methods. Its drawback is that only a few compounds exhibit this effect because (1) the material needs to have a quite low dielectric anisotropy ($|\varepsilon_a| \ll 1$), (2) the concentration of its ionic impurities should be sufficiently low in order to avoid large screening effects, and (3) other phenomena (e.g., EC or Freedericksz transition) should not influence the homogeneous planar initial state below the threshold of FD.

The threshold characteristics for dc driving voltage have long ago been calculated analytically [2] using the one-elastic-constant approximation ($K_{11} = K_{22} = K$)

$$\tilde{U}_{cFD} = \frac{2\pi K}{|e_1 - e_3|(1+\mu)}, \tag{4}$$

$$\tilde{q}_{cFD} = \frac{\pi}{d}\sqrt{\frac{1-\mu}{1+\mu}}, \tag{5}$$

where e_1 and e_3 are the splay and bend flexoelectric coefficients, respectively, and

$$\mu = (\varepsilon_0 \varepsilon_a K)/|e_1 - e_3|^2. \tag{6}$$

According to Eq. (5), the flexodomains can only exist for the material parameter combination $|\mu| < 1$. This leads to the requirement $|\varepsilon_a| < |e_1 - e_3|^2/(\varepsilon_0 K)$ that should be valid for materials showing FDs. Combining Eqs. (5) and (6) yields

$$|e_1 - e_3| = \sqrt{\varepsilon_0 \varepsilon_a K \frac{1+q_{cFD}^2}{1-q_{cFD}^2}}. \tag{7}$$

For 1OO8, both q_{cFD} and U_{cFD} were measured as the function of temperature using 10 mHz ac sine voltage. We assumed that 10 mHz is low frequency enough to be considered as a quasistatic case, hence we have fitted the results with a static model. Therefore, U_{cFD} here is presented in voltage amplitude values instead of rms since FD appears when the driving voltage reaches its maxima. Therefore, U_{cFD} in Fig. 10 is presented in voltage amplitudes instead of rms values.

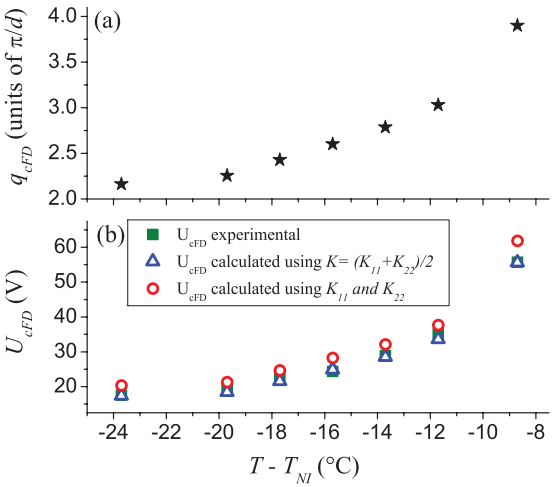

FIG. 10. (Color online) The temperature dependence of (a) the wave number q_{cFD} and (b) the voltage U_{cFD} (amplitude) at the onset of flexodomains.

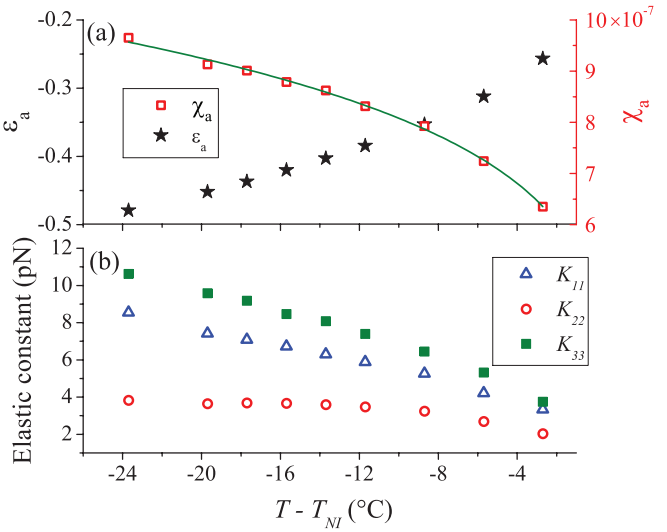

FIG. 11. (Color online) The temperature dependence of (a) the dielectric (ε_a) and the diamagnetic (χ_a) anisotropies, and (b) the three elastic moduli.

Both q_{cFD} and U_{cFD} increase strongly toward higher temperatures. Above $T - T_{NI} = -8$ °C, we could not detect flexodomains up to the voltage of 135 V.

In order to determine $|e_1 - e_3|$, we have measured some material parameters of 1OO8 using methods based on electric and magnetic Freedericksz transitions. The temperature dependence of ε_a and of the diamagnetic susceptibility anisotropy (χ_a) is shown in Fig. 11(a). ε_a is negative and relatively small, as it was expected. Therefore, in our planar sandwich cell geometry the dielectric interaction stabilizes the planar structure; no electric field induced Freedericksz transition occurs. The values and the thermal behavior of χ_a are in the regular range of those in rodlike nematics. This also holds for the elastic constants K_{11}, K_{22}, and K_{33}, which are plotted in Fig. 11(b). We note that K_{33} is shown only for the sake of completeness; we do not use it further on.

The temperature dependence of $|e_1 - e_3|$, presented in Fig. 12, was calculated from the measured data by two different techniques. The first method (square symbols) was based on the analytical formula (7) of the one-elastic-constant

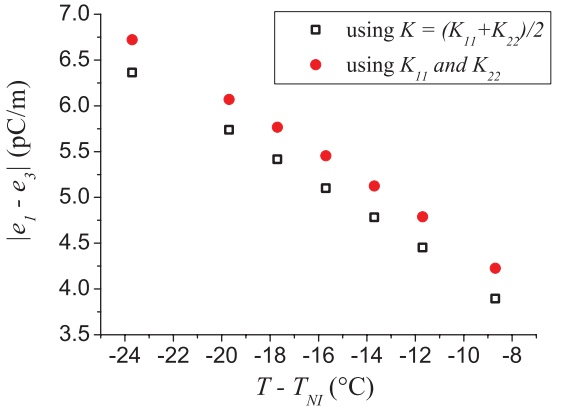

FIG. 12. (Color online) The temperature dependence of the combination $|e_1 - e_3|$ of the flexoelectric coefficients.

approximation, taking $K = (K_{11} + K_{22})/2$. The second technique (triangle symbols) utilized the recent theory [10] of flexoelectric domains that takes into account the anisotropic elasticity ($K_{11} \neq K_{22}$), calculating $|e_1 - e_3|$ numerically. As seen in Fig. 12, the second method provided values about 7% higher than those by the first one; both values of $|e_1 - e_3|$ fall in the regular range of that of rodlike nematics.

In order to check the consistency of our models and the obtained data, we have calculated $U_{c\mathrm{FD}}$ using the $|e_1 - e_3|$ values determined from $q_{c\mathrm{FD}}$. The results, depicted in Fig. 10(b), show that the first model gave about 2% lower, while the second one about 11% higher values for $U_{th\mathrm{FD}}$ than the experiments.

Knowing the temperature dependence of $|e_1 - e_3|$ gave us an opportunity to compare our results with the predictions of the molecular theory of flexoelectricity. It is expected [31–33] that the difference of flexoelectric coefficients should be proportional to the square of the order parameter $S(T)$:

$$|e_1 - e_3| = \hat{e} S^2(T), \tag{8}$$

where the proportionality constant is denoted by $\hat{e}$.

In Fig. 12, $|e_1 - e_3|$ is decreasing with the temperature, which is consistent with the similar tendency of the order parameter. For a more quantitative comparison, the knowledge of $S(T)$ would be essential. $S(T)$ can only be accessed via measuring physical quantities that are directly coupled to it. The diamagnetic susceptibility, which is already determined from the Freedericksz-transition measurements [Fig. 11(a)] is a good candidate since it should be proportional to S [35]:

$$\chi_a(T) = \hat{\chi} S(T), \tag{9}$$

where $\hat{\chi}$ is a constant. In order to determine $\hat{\chi}$ and $S(T)$, the generalized form of the empirical Haller-extrapolation [34,35] method is applied via fitting the experimental data of $\chi_a(T)$ with

$$\chi_a(T) = \hat{\chi} \left(1 - \beta \frac{T}{T_{NI}}\right)^{\gamma}, \tag{10}$$

where β, γ are constants, and the temperature data (T, T_{NI}) are measured in the Kelvin scale. The result of the fit can be seen in Fig. 11(a) (solid line). The parameters of the best fit correspond to $\hat{\chi} = 1.64 \times 10^{-6}$, $\beta = 1$, and $\gamma = 0.2$. Aside from the dimensionless SI quantity of $\hat{\chi}$, its molar version is often used: $\hat{\chi}^M = \hat{\chi} M_m/\rho$, where M_m and ρ are the molar weight and the density, respectively. Using $M_m = 356.5$ g/mol and $\rho = 1$ g/cm^3, one gets $\hat{\chi}^M = 585 \times 10^{-6}$ cm^3/mol, a value that fits well in the range of earlier results [35,36] obtained for different compounds with two aromatic rings.

Combining Eqs. (8) and (9) yields

$$\chi_a = a\sqrt{|e_1 - e_3|}, \tag{11}$$

with $a = \hat{\chi}/\sqrt{\hat{e}}$.

Figure 13 provides a test of this relation, as it plots the measured χ_a values against $\sqrt{|e_1 - e_3|}$ calculated for the same temperatures (determined from the model with anisotropic elasticity). The fit corresponding to Eq. (11), represented by the dashed line, seems to be quite good in spite of the fact that there was only one fit parameter. The best fit results

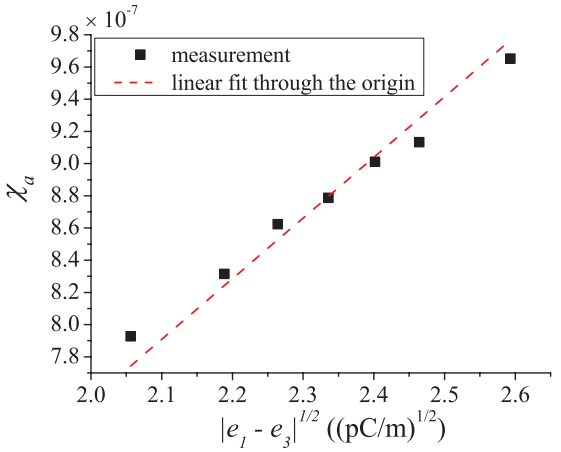

FIG. 13. (Color online) The relation between χ_a and $\sqrt{|e_1 - e_3|}$.

$a = 0.38$ (C/m)$^{-0.5}$, which with $\hat{\chi}$ determined above yields $\hat{e} = 18.6$ pC/m.

IV. CONCLUSIONS

We have investigated the pattern forming phenomena induced by ultralow frequency sinusoidal voltages applied onto the calamitic nematic liquid crystal 1OO8. It was found that the behavior in this low frequency range is characteristically different from that typical for high frequencies: here, patterns appear as flashes in a short time interval within each half period of driving. Two kinds of pattern morphologies were detected: electroconvection rolls and flexodomains. The types of patterns differ in their wave vector (EC rolls are oblique to, while FDs are parallel with, the initial director); moreover, their flashes occur subsequently with a time separation, although in the same (and each) half period of driving. These scenarios are similar to those reported recently [8,9] for the nematic mixtures Phase 5 and Phase 4.

Electric current measurements carried out simultaneously to pattern recording indicated strongly nonlinear current responses: the time dependence of the current showed sharp peaks after each polarity reversal of the applied voltage. The current nonlinearity in 1OO8 was much more pronounced than in Phase 5. This behavior is attributed to the ionic conductivity of the liquid crystal. The transient current may be due to the motion of ions during building up a Debye screening layer at the electrodes, while the (insulating) polyimide coating ensuring the planar alignment blocks the charge transfer through the electrodes.

We found that, interestingly, the time instant of the flashing EC patterns (the time of the EC contrast peak) and that of the electric current peak coincide. This coincidence holds for all voltages, frequencies, and temperatures that we have tested. The shape of the current signal is not affected by the occurrence of EC significantly, indicating that it originates from the more robust ionic effects described above. This is also supported by the fact that the current peaks could be observed below as well as above the EC threshold, and even in the isotropic phase. We think that the current peak has a significant effect on the formation of EC, but not vice versa; the appearance of the EC flashes is synchronized to the current

peaks. Recently, we reported a comparison [9] between the measured and the theoretically calculated time instants of the EC flashes for Phase 5. It indicated that in the experiment at ultralow f, EC occurred earlier within the half period than expected from the extended standard model of EC [6,10]. We suggest that the phase locking of EC to the ionic current peaks might be the reason for this mismatch (the extended standard model does not consider ionic effects). We guess that an adequate extension of the theory to weak electrolytes could reveal this problem and additionally explain the role of the robust current peaks in the pattern formation; proving that, however, represents a great theoretical challenge for the future.

By studying the threshold characteristics of the patterns, we found that the behaviors of EC and FD are essentially different. Flexodomains have a sharp threshold, i.e., the pattern contrast increases suddenly for $U > U_c$. For EC, this holds only at high f; reducing the frequency the EC threshold becomes gradually less sharp (the contrast changes smoothly with the voltage). On the one hand, it hinders the precise determination of the EC threshold. On the other hand, we showed that this tendency can be followed quantitatively using an imperfect bifurcation model. In this approach, the amount of imperfection increases as the frequency is lowered.

EC and FD have different frequency dependencies of their thresholds. At high f, the EC threshold is lower, while at dc driving flexodomains are seen. Therefore, it is not surprising that there is a crossover between EC and FD at around 60 mHz, where their thresholds become equal. Such a scenario was already anticipated from measurements on Phase 5, but could first be demonstrated explicitly now on 1OO8.

Interestingly, the two kinds of patterns can appear in the same half period in some frequency range on both sides of the crossover point, including frequencies where the two thresholds are quite different. This is made possible by the narrow time interval and time separation of the flashes.

The $q_{c\mathrm{EC}}(f)$ curve of 1OO8 shows a discontinuity at $f_c \approx 7$ Hz, indicating a crossover from conductive to dielectric convection rolls. Interestingly, unlike similar crossovers reported at high frequencies in other compounds, here both the conductive and the dielectric rolls are oblique around this crossover frequency; consequently, the Lifshitz frequency is located in the dielectric regime. Although oblique dielectric rolls have already been reported recently in Phase 4 (which had no conductive regime at all) [8], 1OO8 is a substance which exhibits a directly observable transition from oblique conductive to oblique dielectric rolls with increasing the frequency of the ac voltage. The low f_c indicates a fairly low electrical conductivity, which also helps distinguishing between EC and FD patterns by increasing their time separation and may also be responsible for the enhanced nonlinearity of the current.

Measuring the critical wave number of the flexoelectric domains offers a way to calculate the combination $|e_1 - e_3|$ of the flexoelectric coefficients using theoretical models based either on the one-elastic-constant approximation or on a rigourous handling of anisotropic elasticity. It has turned out that the values determined by the two methods differ only by about 7%. The reason for this small difference is that the relevant material parameters (K_{11}, K_{22}, and ε_a) of 1OO8 fall into that range, where $q_{c\mathrm{FD}}$ is only slightly sensitive to the elastic anisotropy. The threshold voltages of FDs, calculated from the theoretical models using the above values of $|e_1 - e_3|$, show a satisfactory agreement with the measured data; this proves the consistency of the models.

In cooling, 1OO8 has a nematic temperature range of about 25°. The temperature dependence of the elastic moduli, the dielectric and the magnetic anisotropies, was determined for the whole nematic range. For $|e_1 - e_3|$, data could be obtained only for the lower temperature part of the nematic phase as flexodomains did not exist for $T - T_{NI} > -8$ °C. The temperature dependence of $|e_1 - e_3|$ was compared with that of χ_a, the latter being proportional to $S(T)$. It was found that $|e_1 - e_3| \propto S^2$ is satisfied, as it is expected from the molecular theory of dipolar flexoelectricity, and also the proportionality constant was determined.

ACKNOWLEDGMENTS

Financial support by the Hungarian Research Fund OTKA K81250 is gratefully acknowledged. We also thank W. Pesch for fruitful discussions.

[1] L. M. Blinov and V. G. Chigrinov, *Electrooptic Effects in Liquid Crystal Materials* (Springer, New York, 1996).

[2] Yu. P. Bobylev and S. A. Pikin, Zh. Eksp. Teor. Fiz. **72**, 369 (1977) [Sov. Phys.–JETP **45**, 195 (1977)].

[3] Á. Buka, N. Éber, W. Pesch, and L. Kramer, in *Self Assembly, Pattern Formation and Growth Phenomena in Nano-Systems*, edited by A. A. Golovin and A. A. Nepomnyashchy (Springer, Dordrecht, 2006), pp. 55–82.

[4] Á. Buka, N. Éber, W. Pesch, and L. Kramer, Phys. Rep. **448**, 115 (2007).

[5] E. Bodenschatz, W. Zimmermann, and L. Kramer, J. Phys. (Paris) **49**, 1875 (1988).

[6] A. Krekhov, W. Pesch, N. Éber, T. Tóth-Katona, and Á. Buka, Phys. Rev. E **77**, 021705 (2008).

[7] M. Treiber and L. Kramer, Mol. Cryst. Liq. Cryst. **261**, 311 (1995).

[8] M. May, W. Schöpf, I. Rehberg, A. Krekhov, and Á. Buka, Phys. Rev. E **78**, 046215 (2008).

[9] N. Éber, L. O. Palomares, P. Salamon, A. Krekhov, and Á. Buka, Phys. Rev. E **86**, 021702 (2012).

[10] A. Krekhov, W. Pesch, and Á. Buka, Phys. Rev. E **83**, 051706 (2011).

[11] L. Kramer and W. Pesch, in *Pattern Formation in Liquid Crystals*, edited by Á. Buka and L. Kramer (Springer, New York, 1996), pp. 221–256.

[12] L. Kramer and W. Pesch, in *Physical Properties of Nematic Liquid Crystals*, edited by D. A. Dummur, A. Fukuda, and G. R. Luckhurst (Inspec, London, 2001), pp. 441–454.

[13] E. Kochowska, S. Németh, G. Pelzl and Á. Buka, Phys. Rev. E, **70**, 011711 (2004).
[14] Á. Buka, T. Tóth-Katona, N. Éber, A. Krekhov, and W. Pesch, in *Flexoelectricity in Liquid Crystals. Theory, Experiments and Applications*, edited by Á. Buka and N. Éber (Imperial College Press, London, 2012), pp. 101–135.
[15] M. Majumdar, P. Salamon, A. Jákli, J. T. Gleeson, and S. Sprunt, Phys. Rev. E, **83**, 031701 (2011).
[16] G. G. Nair, C. A. Bailey, S. Taushanoff, K. Fodor-Csorba, A. Vajda, Z. Varga, A. Bóta, and A. Jákli, Adv. Mater. **20**, 3138 (2008).
[17] S. Rasenat, G. Hartung, B. L. Winkler, and I. Rehberg, Exp. Fluid **7**, 412 (1989).
[18] G. Derfel, J. Mol. Liq. **144**, 59 (2009).
[19] F. C. M. Freire, G. Barbero, and M. Scalerandi, Phys. Rev. E **73**, 051202 (2006).
[20] F. C. Freire, A. L. Alexe-Ionescu, M. Scalerandi, and G. Barbero, Appl. Phys. Lett. **89**, 214101 (2006).
[21] G. Barbero, A. M. Figueiredo Neto, F. C. M. Freire, and J. Le Digabel, Phys. Rev. E **74**, 052701 (2006).
[22] G. Barbero, G. Cipparrone, O. G. Martins, P. Pagliusi, and A. M. Figueiredo Neto, Appl. Phys. Lett. **89**, 132901 (2006).
[23] A. L. Alexe-Ionescu, G. Barbero, and I. Lelidis, Phys. Rev. E **80**, 061203 (2009).
[24] L. O. Palomares, J. A. Reyes, and G. Barbero, Phys. Lett. A **333**, 157 (2004).
[25] R. Atasiei, A. L. Alexe-Ionescu, J. C. Dias, L. R. Evangelista, and G. Barbero, Chem. Phys. Lett. **461**, 164 (2008).
[26] G. Barbero, F. Batalioto, and A. M. Figueiredo Neto, Appl. Phys. Lett. **92**, 172908 (2008).
[27] S. P. Trainoff and D. S. Cannell, Phys. Fluids **14**, 1340 (2002) and references therein.
[28] W. Pesch (private communication).
[29] A. Hertrich, A. P. Krekhov, and W. Pesch, J. Phys. II **5**, 733 (1995).
[30] T. Tóth-Katona, N. Éber, Á. Buka, and A. Krekhov, Phys. Rev. E **78**, 036306 (2008).
[31] W. Helfrich, Z. Naturforsch. **26A**, 833 (1971).
[32] A. Derzhanski and A. G. Petrov, Phys. Lett. A **36**, 483 (1971).
[33] M. A. Osipov, in *Flexoelectricity in Liquid Crystals. Theory, Experiments and Applications*, edited by Á. Buka and N. Éber (Imperial College Press, London, 2012), p. 932.
[34] F. Leenhouts, W. H. de Jeu, and A. J. Dekker, J. Phys. (France) **40**, 989 (1979).
[35] R. Stannarius, in *Handbook of Liquid Crystals*, edited by D. Demus, J. Goodby, G. W. Gray, H. W. Spiess, and V. Vill (Wiley-VCH, Weinheim, 1998),Vol. 2A, pp. 113–127.
[36] I. H. Ibrahim and W. Haase, J. Phys. Colloques **40**, C3-164, (1979).